X-ray focusing with lobster-eye optics: a comparison of theory with experiment

A. G. Peele, K. A. Nugent, A. V. Rode, K. Gabel, M. C. Richardson, R. Strack, and W. Siegmund

We report an experimental investigation and comparison with simulation of the x-ray focusing of a flat, square profile microchannel plate. We use x rays with an energy of ~1.5 keV from a laser-produced plasma. The images were recorded with x-ray film. We find the focal structure to be consistent with theoretical expectations. The angular resolution of the focus is 0.96 mrad, which is a major improvement over previous results. The measured peak intensity gain is 27 ± 4, which is ~33% of that for a perfect optic. © 1996 Optical Society of America

1. Introduction

X-ray optics based on either single or multiple capillaries have received considerable interest over the past few years. Single capillary optics have been developed for microanalysis and microfluorescence studies with synchrotron and laboratory x-ray sources,[1] and multiple capillaries arrays such as the Kumakhov lens[2] have been investigated. A related but separate field of development is that of the microchannel plate (MCP), or lobster-eye, x-ray optic.[3] The MCP can be either flat or curved. The MCP may have a high numerical aperture, and it has a real image, whereas a mirror of equal radius would have a virtual image.[4]

Workers in x-ray astronomy[5,6] have taken a particular interest in the development of the MCP because when it is curved into a spherical geometry and square profile channels are used, it becomes equivalent to the so-called lobster-eye telescope first proposed by Angel[7] and is closely related to the orthogonal mirror proposed by Schmidt.[8] Chapman *et al*.[9] published an exhaustive theoretical treatment of the properties of square channel arrays. A telescope based on these lines will have a very wide field of view and excellent sensitivity.[10]

To reach their capabilities, MCP's must be manufactured accurately to reduce figure error and have low surface roughness to reduce scattering. Their being manufactured from or coated in a material with high x-ray reflectivity is also desirable. Initial investigations of MCP's[5,6] have used flat samples because figure error and surface roughness can be readily evaluated and samples are easier to prepare.

The cruciform structure of the focal spot for square profile channels was observed in the x-ray region for the first time by Fraser *et al*.,[11] though the focal spot was itself somewhat broader than was expected because of imperfections in the MCP. In this paper we report cruciform focal structures that are closer to the theoretical predictions than previously observed. However, the overall efficiency is still somewhat diminished. Based on the results of our simulations we believe this diminution in efficiency is due mainly to channel rotations and twists and also to surface roughness. We find that losses due to channel tilts are negligible. With these effects incorporated into the model, excellent agreement was found between theory and experiment. Accordingly, the MCP is rapidly evolving toward becoming a useful and practical x-ray optical device.

2. Principle of Operation

The principal of the lobster-eye lens is based on the visual system of macruran crustaceans (lobsters, shrimps, and crayfish)[12] and has been discussed a number of times in other publications.[3–7] The central idea is illustrated in Fig. 1(a), where, for a one-dimensional lens, an array of mirrors will bring a

A. G. Peele and K. A. Nugent are with the University of Melbourne, Parkville, Victoria 3052, Australia. A. V. Rode is with the Australian National University, GPO Box 4, Canberra City, ACT 2601, Australia. K. Gabel and M. C. Richardson are with the University of Central Florida, Orlando, Florida 32826. R. Strack and W. Siegmund are with Schott Fiber Optics Inc., Southbridge, Massachusetts 01550-1960.

Received 13 July 1995; revised manuscript received 4 March 1996.

0003-6935/96/224420-06$10.00/0

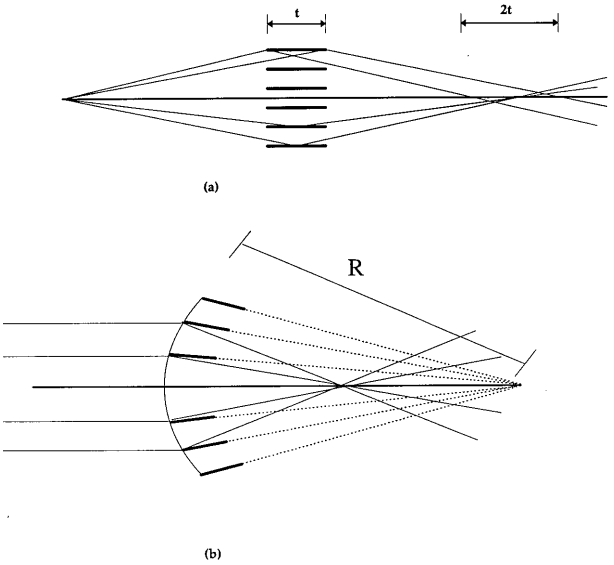

Fig. 1. (a) Principle of one-dimensional focusing, point to point. Focal aberration is due to channel length. (b) One-dimensional focusing for a distant object.

point source of x rays to a focus. Note that here we depict a flat array. To focus a distant object, the array must be curved, as in the case of a lobster eye, so that the reflecting planes have a common center of curvature [see Fig. 1(b)]. In two dimensions the x rays need to be reflected from a surface perpendicular to that shown in Fig. 1, and so an array of square channels will bring the radiation to a focus in two dimensions. In the case when the array is bent to a spherical surface, as in a lobster eye, the optic has no preferred axis and so is able to focus equally well in all directions. It is this property that makes the lobster eye a candidate for a wide-field-of-view telescope.

The focusing performance of the MCP may be effectively understood with the theoretical results published by Chapman *et al*.[9] The MCP consists of an array of square channels. Those x rays that strike the exterior walls on the face of the MCP are lost. Of the x-ray photons that enter a channel, a fraction that reflect once off two orthogonal walls are reflected into the focal spot, another fraction are reflected only from one wall and so are focused in one dimension to a line passing through the two-dimensional focus, and a third fraction pass straight through the array to form an unfocused background. Higher-order reflections are also possible, but the x-ray photons from such reflections strike a detector as if they were in one of the above classes. The resulting focal structure then consists of a bright focused spot with a fainter cross centered on this and a much less intense diffuse background. The relative number of photons in each of the above structures depends on the ratio of the width of the channels to their length. At the optimal ratio for a lens with no axis of symmetry and with 100% reflectivity, 34.3% of the photons are focused into the central square, 24.3% end up in each of the one-dimensional foci (arms), and 17.2% end up in the unfocused background. The focusing efficiency in a given direction may be improved when a preferred axis is imposed on the device,[9] but this is not consistent with a very-wide-field-of-view telescope.

Table 1. Summary of the Production Method for Microchannel Plates

MCP Manufacturer Procedure
Grind and polish square acid-soluble core bar
Place core bar inside lead-glass tubing
Draw square monofibers
Assemble square array of several square monofibers
Draw square multifibers
Assemble square array of several square multifibers inside glass tube
Draw tube of multifibers to final square cross section
Anneal the square boule
Slice, grind, and polish plates from the annealed square boule
Acid etch plates to remove core
Additional chemical processing if necessary

The x rays are brought to a focus with an angular resolution comparable with the angle that an individual channel subtends at the detector. In practice this implies that the lobster-eye telescope will always be limited in resolution by the physical size of the individual channels. This also leads us to the conclusion that the lobster-eye's promise in x-ray astronomy is primarily as an all-sky x-ray monitor. As a true focusing device, the lobster-eye will be able to image objects very effectively against the diffuse sky background and so may allow the observation of the time history of objects that are undetectable by current all-sky monitors.[10]

3. Experimental Arrangement

The MCP's used in our experiment were manufactured by Schott Fiber Optics. Proprietary techniques were used to treat the acid-soluble core bar and in the etching procedure. These techniques ensure that channels exhibit a high degree of squareness and reduce etching time, thereby, in principle, reducing surface roughness in the etched channels. With the exception of these techniques, our MCP's were manufactured with standard methods of MCP manufacture and with particular attention to the squareness of the channels. The general procedure for manufacture of MCP's has been discussed elsewhere[13] and is summarized here in Table 1.

A micrograph of the MCP used is shown in Fig. 2. Each MCP we investigated was 1.5 cm square; the channel side length was 200 μm, and the channel length was 6 mm. Wall thickness was 40 μm. The MCP's were mounted on a two-axis adjustable stage with a source–MCP and MCP–film distance of 237 mm. The source, MCP, and film were all inside an evacuated chamber (see Fig. 3). The x rays were generated with a laser-produced plasma created by a 17-ns, 17-J pulse of laser radiation ($\lambda = 1.064$ nm) that was focused through an $F/10$ lens onto a copper target inside an evacuated chamber. The focal spot

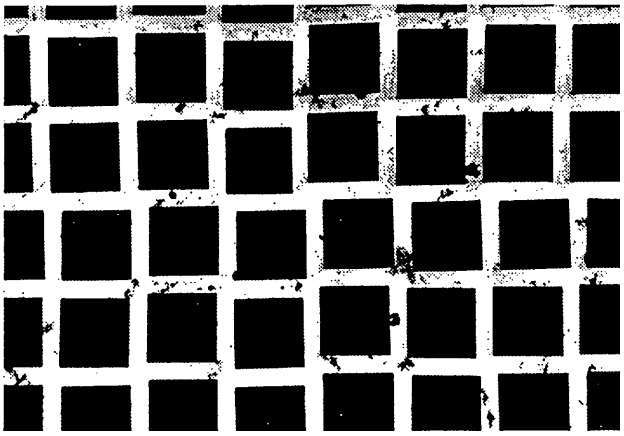

Fig. 2. Optical micrograph of our MCP.

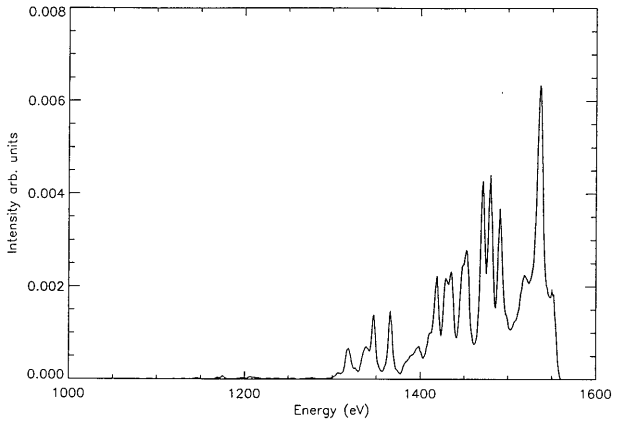

Fig. 4. Transmitted intensity spectrum through 60-μm Al filter. The spectrum was taken to be monoenergetic at an energy of 1.5 keV in our analysis.

was ~150 μm in diameter. This provides a flux density from the laser on the target surface of order 10^{13} W/cm^2 and produces a plasma that is an intense source of x rays in the energy range 1–1.6 keV with a conversion efficiency as high as 60%.[14]

Images were recorded on Kodak DEF x-ray film. The film was developed and fixed by the procedure given by Henke *et al.*[15] To measure intensity, a Joyce–Loebls densitometer with matched NA = 0.1 optics was used to record the optical density of the film. The results given by Henke *et al.*[15] were then used to calculate the intensity. Aluminium foil was used as a filter to protect the x-ray film from visible light.

Figure 4 shows the spectrum measured from the plasma with a flat rubidium hydrogen phthalate crystal with 2*d* spacing, 26.121 Å, and which has been modified to take into account the effect of the 60-μm Al filter. It is clear that more than 90% of the radiation reaching the film is between 1.36 and 1.56 keV, the absorption edge of Al. In analyzing the data, we made the simplifying assumption that the x-ray energy was monochromatic with an energy of 1.5 keV.

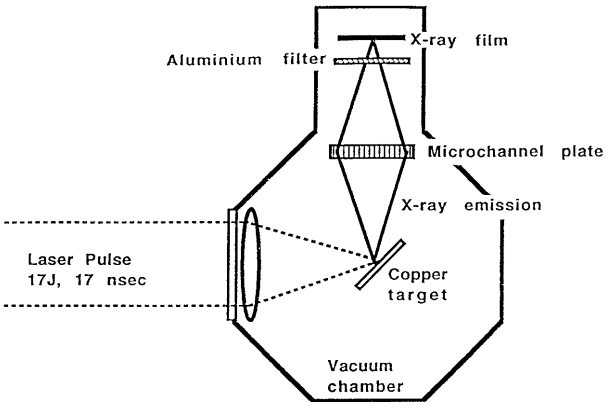

Fig. 3. Schematic of the experimental layout. The laser pulse is focused onto the copper target that produces a plasma. The x-ray emission is then focused by the MCP onto the x-ray film.

4. Results

Figure 5 shows the x-ray photograph of the focal plane. The checkerboard pattern that is due to shading by channel walls in the MCP can be clearly seen. The expected focal distribution is also observed. While there is some flaring along the focal arms, the effect is relatively small. This indicates that the MCP is extremely well produced. Some channel irregularities can also be observed.

Figure 6 shows a one-dimensional intensity trace taken along one of the focal arms. The full width at half-maximum (FWHM) of the central focus is 230 μm compared with 200 μm expected for a geometrically perfect MCP. If we define the angular resolution to be the central focus FWHM divided by the image distance, the angular resolution is therefore very close to that for a perfect MCP that is fixed by the channel size and object distance alone. We observe a resolution of 0.96 mrad, which compares with 0.84 mrad for a perfect MCP. This is the best resolution yet reported for an MCP.

A second prime indicator of the quality of an MCP is the efficiency with which the radiation is brought to the focus. A section of the film was exposed directly to the source, enabling us to estimate the intensity of the unfocused flux. We define the ratio of the inten-

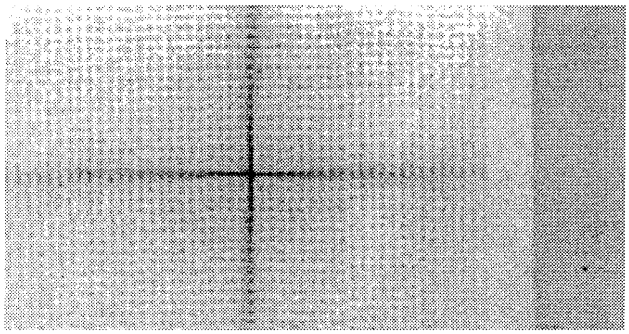

Fig. 5. Photograph of focal distribution produced by the MCP optic.

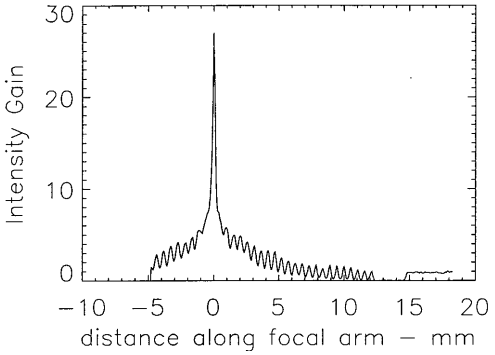

Fig. 6. One-dimensional scan, along a focal arm, of intensity gain.

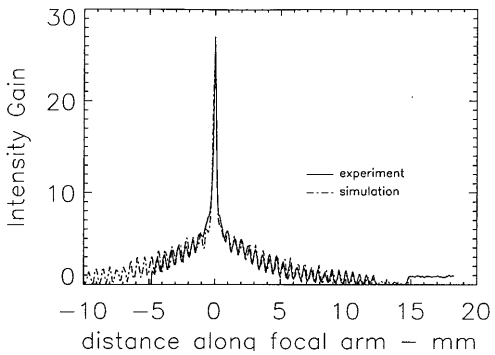

Fig. 7. Simulated intensity along a focal arm overlaid onto the data in Fig. 6. The agreement is excellent.

sity of the focused flux to the intensity of the unfocused flux as the intensity gain. The intensity gain figure thus calculated can be compared with the theoretical intensity gain that would be obtained with realistic reflectivity estimates for a geometrically perfect and perfectly smooth MCP. We compare both peak intensity gain and average intensity gain over the FWHM of one focal arm. Peak intensity gain is the peak gain recorded in a collection area equal to the slit size of the densitometer used to record the optical density—in our case, 100 μm. The average intensity gain over the FWHM of one focal arm is the average gain for a one-dimensional scan along one of the focal arms with the same collector size as that used in the peak measurement.

We measure the peak intensity gain in the central focus to be 27 ± 4, while the average intensity gain over the FWHM of one focal arm of the focal region is 21 ± 4. The expected peak intensity gain was calculated by a Monte Carlo ray-tracing simulation, for a perfect MCP for the experimental parameters, and was found to be 83. The average intensity gain over the FWHM of one focal arm for a perfect MCP was 62.

5. Analysis

Obvious departures from the expected intensity distribution for a perfect MCP are reduction and broadening of the central peak and the diminution in intensity along the focal arms. These departures can be explained by a simple model of surface roughness, channel rotation, channel twisting, and nonsquareness and channel tilt.

Surface roughness reduces the intensity in the reflected beam and hence in the focus. Flux is also scattered away from the direction of the specular beam because of surface roughness.[16] We use the Debye–Waller factor[17,18] with σ equal to the rms roughness to calculate the reduction in intensity in the specularly reflected beam. For the purpose of this model we take no account of diffusely scattered x rays, simply treating such rays as lost. If diffuse scattering is significant, it would be expected to be most noticeable as a low-intensity halo about the central peak. In Fig. 7 a small amount of residual broadening at the base of the central peak can in fact be observed. It should also be kept in mind that the nonsquareness (or twist) parameter described below mimics to some extent the effect of diffuse scattering, and as such the value derived for this parameter may be overstated.

Rotation of a channel about the long axis of the channel by a certain amount has the effect of rotating the flux distribution from that channel by an equal amount. Consequently the focal square will tend to become circular and the focal arms will flare out. The effect in measured intensity is therefore greatest in the focal arms, causing intensity to drop off dramatically along the arms. In the focal square this effect is of less consequence. We characterize rotations as normally distributed with a rms rotation equal to ϕ. For the purpose of this model we take no account of the fact that, on observation, channel rotations appear to be correlated with fiber bundles within the MCP.

Channel tilt about either of the two axes that are perpendicular to the long axis of the channel causes the reflected ray to deviate by twice the tilt. This will appear as a blur in the image. The central focus will be particularly affected, as there are two reflections for centrally focused rays. We characterize tilts along the optic axis as normally distributed with rms tilt equal to ξ.

If a channel is nonsquare, then the second reflection will not be orthogonal to the first. Hence the central focus will be broadened and the focal arms will flare out. Channel twisting will cause the same effect. This effect is to be distinguished from channel rotation that causes flare and only minor central focus broadening and from channel tilt that causes broadening in both the central and arm foci. We were led to the inclusion of this parameter by an inability to fit the observed intensity distribution with the other parameters alone (although note the previous comments regarding diffuse scattering). We characterize the combined effect of the twist and nonsquareness by a normally distributed distribution in deflection angle with rms equal to η.

These parameters were incorporated into a ray-tracing simulation that takes account of the real reflectivity on reflection. The experimentally fixed variables described in Section 3 were included, and

intensities in pixels corresponding to the resolution of the film densitometer were obtained.

Each of the geometric parameters ξ, ϕ, η and the surface roughness σ has a unique effect on the shape of the observed intensity distribution. Accordingly it is possible to obtain reasonably good agreement with the experimental data by varying the appropriate parameters individually to match the data. It did not appear possible to obtain a similarly close fit with a grossly different set of parameters. This is to be expected because of the independent effect of each of the parameters. Once a reasonable approximation was reached by eye, a least-squares search based on the Levenberg–Marquardt method[19] was used to obtain a best fit for the parameters. This method requires the estimation of the partial derivatives of the χ^2 value with respect to the parameters. As we use a simulation based on a ray-trace calculation to model the data, there is a trade off between the amount of noise induced by the simulation and the time taken to evaluate the simulation. We opted for a simulation that traces the trajectories of 10^6 rays. At this level of noise the algorithm consistently converged to values within 10% of those stated below. When random starting values were used, the algorithm either converged to a local minimum with a significantly worse χ^2 than the best fit or was within 10% of the best fit for each of the parameters. Accordingly we quote the fitted parameters to no better than 10%. However, it is still possible to identify which defects have a large effect on the performance of the MCP.

The best-fit results were $\sigma = 2.4$ nm, $\phi = 20$ mrad, $\eta = 35$ mrad, and $\xi = 0.05$ mrad. At this magnitude the effect of channel tilt is negligible in the simulation, and the surface roughness accounts for a loss in intensity of only $\sim$25%, assuming an average angle of reflection of 15 mrad.

Figure 7 shows the result of the ray-tracing simulation overlaid onto the experimental result shown in Fig. 6. The simulation is in excellent agreement with the measurement. Importantly, the simulation suggests that the major factor in reducing intensity in the central focus is not channel tilts but a combination of channel rotations and twist and, to a lesser extent, surface roughness.

Figure 7 demonstrates that we are able to model the performance of an MCP accurately with the simple model discussed above. However, because of the simplifications in the model we might expect there to be some difference between the fit parameters and those measured directly.

6. Comparison with Direct Metrology

We measured the surface of the channel interior walls by using a Western Digital Nanoscope 3, atomic force microscope. On a scale of $\sim$30 μm, striations running along the length of a channel similar to those reported by Kaaret *et al.*[6] could be observed. We measured along the channel length on a scale of $\sim$1 μm and found the rms roughness to be $\sim$2 nm. Although this is in qualitative agreement with the fit value, the rms roughness can be considerably different on different length scales or if measured in a different direction. The difficulty of obtaining accurate measurements by this method without additional calibration and investigation of the atomic force microscope and the sample is also noted. To obtain accurate results, the structure in the roughness over various length scales and the effects of diffuse scattering will probably be required.

We observe rotations within a fiber bundle and between adjacent fiber bundles, as has been reported elsewhere,[20] in our case at $\sim$17 mrad and $\sim$20 mrad, respectively. This is also in good agreement with the simulation parameter. However, it is likely that for accurate comparison a more detailed model should be used. In this case the distribution of rotations, including the correlation of rotation with fiber bundles, should be included.

Measurements of the nonsquareness of the channels from observations of the face of the MCP suggest a deviation from square of order 5 mrad rms or less. Accordingly we propose that it is channel twist that is a major contributor to the overall imperfection of the MCP. At this stage we have not attempted to measure the channel twist directly.

As an independent measure of the combined effect of the rms rotation and the twist, we measured the flare angle along a focal arm. A rotated MCP will have arms rotated by the same amount. Accordingly, with the FWHM of the focal arm measured at successive distances from the central focus, the flare angle and hence the combined rms rotation and twist can be calculated. This method gives us an estimate of 74 mrad rms angular deviation, which is in qualitative agreement with the total of rotation and twist of 55 mrad obtained from the simulation.

We have not attempted any direct measurement of channel tilts. However, channel tilt appears to be negligible from the simulation.

7. Conclusion

We record peak and average intensity gains of $\sim$33% of that expected for a perfect MCP. We attribute this to the manufacturing process, which appears substantially to eliminate radiusing of channel corners[21] and to reduce problems that are due to surface roughness. Based on the results of our simulations, most of the losses appear to arise from a combination of channel rotations and twists. This gives manufacturers a new problem to address in MCP manufacture. In addition, the resolution of the x-ray focus, 0.96 mrad, is very close to the theoretical ideal of 0.84 mrad. Previous results are 1.9 mrad with a channel size of 86 μm[11] and 3.5 mrad with a channel size of 11 μm.[21] The theoretical resolutions obtainable in both of those cases are 0.12 and 0.016 mrad, respectively. Our results show good promise for the realization of Angel's lobster-eye telescope, if similar performance can be translated into a spherical geometry. We have also demonstrated the ability to model observed results in terms of a simplified model of surface roughness, channel rotations, tilts, and

twists. This model gives us reasonable agreement with direct measurements of those parameters and, to first order, should serve as a useful predictive tool for the performance of future MCP's.

We acknowledge the support of a research grant from the Australian Research Council and support from the Department of Industry Science and Technology. A. G. Peele acknowledges the support of a Commonwealth postgraduate research award.

References

1. E. A. Stern, Z. Kalman, A. Lewis, and K. Lieberman, "Simple method for focusing X-rays using tapered capillaries," Appl. Opt. **27,** 5135–5139 (1988).
2. M. A. Kumakhov and F. F. Komarov, "Multiple reflection from surface x-ray optics," Phys. Rep. **191,** 289–350 (1990).
3. S. W. Wilkins, A. Stevenson, K. Nugent, H. N. Chapman, and S. Steenstrup, "On the concentration, focusing and collimation of x-rays and neutrons using microchannel plates and configurations of holes," Rev. Sci. Instrum. **60,** 1026–1036 (1989).
4. H. N. Chapman and A. V. Rode, "Geometric optics of arrays of reflective surfaces," Appl. Opt. **33,** 2419–2436 (1994).
5. G. W. Fraser, J. E. Lees, J. F. Pearson, M. R. Sims, and K. Roxburgh, "X-ray focusing using microchannel plates," in *Multilayer and Grazing Incidence X-ray/EUV Optics*, R. B. Hoover, ed., Proc. SPIE **1546,** 41–52 (1992).
6. P. Kaaret, P. Geissbuhler, A. Chen, and E. Glavinas, "X-ray focusing using microchannel plates," Appl. Opt. **31,** 7339–7343 (1992).
7. J. R. P. Angel, "The lobster-eye telescope," Astrophys. J. **233,** 364–373 (1979).
8. W. K. H. Schmidt, "A proposed x-ray focusing device with wide field of view for use in x-ray astronomy," Nucl. Instrum. Methods **127,** 285–292 (1975).
9. H. N. Chapman, K. A. Nugent, and S. W. Wilkins, "X-ray focusing using square channel capillary arrays," Rev. Sci. Instrum. **62,** 1542–1561 (1991).
10. W. C. Priedhorsky, A. G. Peele, and K. A. Nugent, "X-ray all-sky monitor with extraordinary sensitivity," Mon. Not. R. Astron. Soc. **279,** 733–750 (1996).
11. G. W. Fraser, A. N. Brunton, J. E. Lees, J. F. Pearson, and W. B. Feller, "X-ray focusing using square pore microchannel plates: first observation of cruxiform image structure," Nucl. Instrum. Methods A **324,** 404–407 (1993).
12. See, for example, M. F. Land, "Animal eyes with mirror optics," Sci. Am. **239** (**6**)**,** 88–99 (1978).
13. See, for example, M. Lampton, "The microchannel image intensifier," Sci. Am. **245** (**5**)**,** 46–55 (1981).
14. C. D. Hendricks, ed. *Laser Program Annual Report*, Rep. UCRL-50021-82 (Lawrence Livermore National Laboratory, Livermore, Calif., 1983) pp. 5–35.
15. B. L. Henke, J. Y. Uejio, G. F. Stone, C. H. Dittmore, and F. G. Fujiwara, "High-energy x-ray response of photographic films: models and measurement," J. Opt. Soc. Am. B **3,** 1540–1550 (1986).
16. Y. Yoneda, "Anomalous surface reflection of x-rays," Phys. Rev. **131,** 2010–2013 (1963).
17. P. Debye, "Interference of Röntgen rays and heat motions," Ann. Phys. **43,** 49–95 (1914).
18. P. Beckmann and A. Spizzichino, *The Scattering of Electromagnetic Waves from Rough Surfaces* (Pergamon, New York, 1963).
19. W. H. Press, S. A. Teukolsky, W. T. Vetterling, and B. P. Flannery, *Numerical Recipes in Fortran: the Art of Scientific Computing*, 2nd ed. (Cambridge U. Press, Cambridge, 1986).
20. G. W. Fraser, A. N. Brunton, J. E. Lees, J. F. Pearson, R. Willingale, D. L. Emberson, W. B. Feller, M. Stedman, and J. Haycocks, "Development of microchannel plate (MCP) x-ray optics," in *Multilayer and Grazing Incidence X-ray/EUV Optics III*, R. B. Hoover and A. B. C. Walker, Jr., eds, Proc. SPIE **2011,** 215–226 (1993).
21. A. N. Brunton, G. W. Fraser, J. E. Lees, W. B. Feller and P. L. White, "X-ray focusing with 11μm square pore microchannel plates," in *X-ray and Ultraviolet Sensors and Applications*, R. B. Hoover and M. B. Williams, eds, Proc. SPIE **2519,** 40–49 (1995).